Conference Paper

Low Liquid-to-solid Ratio of Mining Waste and Slag Binary Alkali-activated Material

Naim Sedira and João Castro-Gomes

Centre of Materials and Building Technologies (C-MADE/UBI), Department of Civil Engineering and Architecture, University of Beira Interior (UBI), 6201-001 Covilhã, Portugal

Abstract

This study investigates the effect of the increasingly compressing pressures on the properties of the low liquid-to-solid (L/S) ratio binary alkali-activated binder to use as a binder for the manufacturing of engineered stones. The binders were a combination of two types of wastes (aluminosilicate source) as precursors (TMWM 50 Vt.% + EAF-Slag 50 Vt.%), blended with (11.11 wt.%) alkaline activator solution (NaOH/Na_2SiO_3 with weight ratio 4/1). The mixtures were molded in cube and exposed to five different pressures (20, 40, 60, 80 and 100 MPa) in order to obtain a compressed alkali-activated binder. The main evaluation techniques in this study were compressive strength, and Fourier Transform Infrared Spectroscopy (FTIR). The results showed that the maximum compressive strength (50.57 MPa) was obtained at a pressing pressure 100 MPa at twenty-eight days of testing.

Corresponding Author:
Naim Sedira
sedira.naim@ubi.pt

1. Introduction

Globally, the construction sector (in particular production of cement) has grown significantly in the last decades, and become the third-largest source of anthropogenic emissions of CO_2 after fossil fuel power plants, and land-use change [1]. In addition, 15% of the indirect CO_2 emissions from non-energy use is emitting from the cement industry. Besides, its production process consumes a huge amount of energy [2]. For this reason, nowadays there is a growing demand to replace cement by alkali-activated materials. These innovative construction materials under certain conditions have lower greenhouse gas emissions, environmental impacts and CO_2 emission associated with their manufacture [3]. Alkaline activation involves a chemical reaction between solid aluminosilicate oxide oxides (Al-Si) and alkali metal silicate MOH solutions (M = alkali metal), (e.g., NaOH, or KOH) under highly alkaline conditions yielding amorphous to semi-crystalline three-dimensional polymeric structures, which consist of Si–O–Al bonds [4–5]. The replace of conventional cement by alkali-activated materials seems to be a potential solution to reduce the CO_2 emissions and environmental risk, such as

contamination of soil, water and air pollution in the surrounding areas. For this, many studies conducted in order to re-use the mineral wastes as aluminosilicate rich source materials [6], such as mining waste [7–8], waste glass [9], red clay brick waste [10] and by-product wastes (such as Fly ash [11] and slag [12]). Among the above-mentioned mineral wastes, slag deserves a special attention in the alkali-activation field and classified as one of the three most commonly used precursors [3–13].

A large quantity of steel slag is the result of main by-products coming from the steel industry. The electric arc furnace (EAF) slag has a similar steel refining process but uses high-power electric arcs to produce high quality steel from recycled steel scrap [14]. The strength and level of the other engineering properties of conventional cement depend on the water-to-cement (*w/c*) ratios used to prepare the mixture. Additionally, strengths, durability and the quality of the other engineering properties of the cementitious materials decrease with the increase of (*w/c*) ratios. However, the decrease of the (*w/c*) ratios had a negative effect on the quality of formed composite properties such as the decrease in the workability of the fresh composite mixtures. It was found that the combination between very low (*w/c*) ratios and pressure compaction enhanced the quality of acquired engineering properties of the composites [15].

The main objectives of this paper were to demonstrate the effect of the intensification of compressing pressure (20, 40, 60, 80, 100 MPa) on the compressive strength results and the formation of aluminosilicate phases after the alkaline activation. Investigation of the hardened low liquid-to-solid binary TMWM-EAF-Slag alkali-activated material will be carried out using FTIR.

2. Materials, Mixture Compositions, and Test Specimens

2.1. Materials

2.1.1. Precursors

Tungsten mining waste mud (TMWM) and electric arc furnace slag (EAF-Slag) were used in this study to prepare a low liquid-to-solid binary TMWM-EAF-Slag alkali-activated material. The TMWM was derived in powder form from the Panasqueira mine in Covilha, Portugal. However, EAF-slag was received in aggregate form from the national steel industry at Maia and Aldeia de Paio Pires, Seixal, Portugal.

The TMWM was sieved under 500 μm, this particle size was used to make alkali-activated materials in many studies that used TMWM as a precursor [8–16]. However,

EAF-Slag was sieved under 45 µm, this particle size was the optimum size for the research of reusing EAF-Slag in cured Clinker-free CO_2 construction materials [17].

The bulk powder densities of TMWM and EAF-Slag were determined using a gas displacement pycnometer (AccuPyc1340, Micromeritics, Norcross, Georgia) and were determined as 3.03 and 3.77 g/cm^3, respectively. The Blaine fineness of the different powders is determined according to EN 196–6, by using (ACMEL LABO BSA1 apparatus), and were determined as 1017 and 5290 cm^2/g, respectively. Moreover, the particle size distribution of the powders (TMWM and EAF-Slag) were subjected to a particle size analysis using laser diffraction (CILAS, 1190) in Fig 1, the TMWM with a mean particle size (d_{50}) is 145.8 µm, while EAF-Slag (d_{50}) is 13.1 µm.
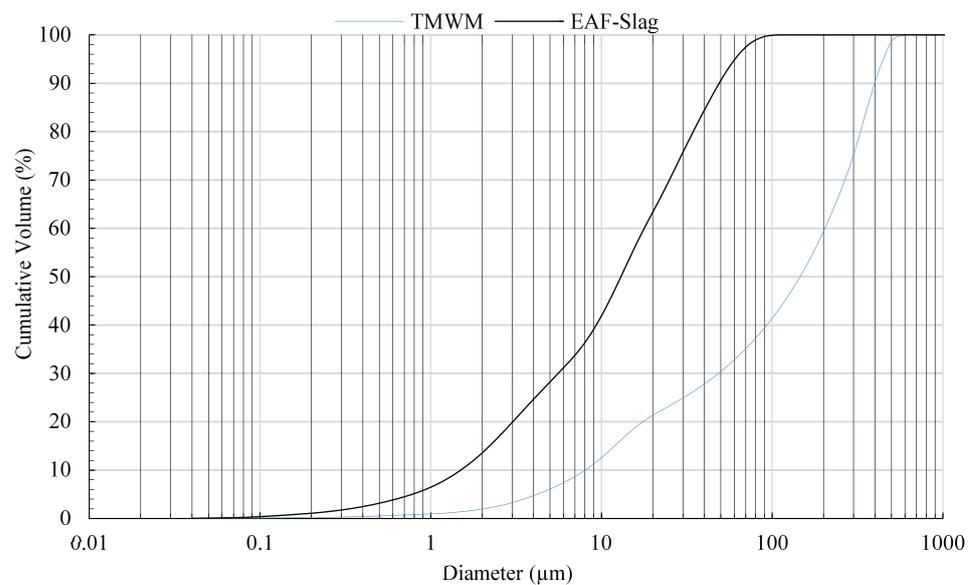
Figure 1: Particle size distribution: cumulative and volume fraction of TMWM and EAF-Slag.

The chemical composition of TMWM and EAF-Slag was determined by Energy-dispersive X-ray spectroscopy (SEM-EDX) using HITACHI S–3400N. The main chemical compositions of TMWM are (SiO_2; 46.7 wt.%), (Al_2O_3; 17 wt.%) and (Fe_2O_3; 15.5 wt.%). The main chemical composition of EAF-Slag (CaO; 33.3 wt.%), (Fe_2O_3; 30.5 wt.%), (SiO_2; 15 wt.%) and (Al_2O_3; 10.1 wt.%), as listed in Table 1.

The X-ray powder diffraction using "Rigaku model D-MAX III/C" to identify the patterns of the raw TMWM and EAF-Slag, the XRD pattern of both materials are shown in Fig 2. The X-ray spectra of the TMWM shown in Fig 2a, indicates the crystalline nature of TMWM and the presence of crystalline phases which were identified by their characteristic: as follows: muscovite (Ref. PDF#46- 1409), quartz (Ref. PDF#46-1045) and clinochlore (ref. PDF#29-0701). Muscovite is a dioctahedral layered structure in which a sheet of octahedral Al ions is sandwiched between two sheets of linked SiO_4 tetrahedral

with a general formula $KAl_2(Si_3Al)O10(OH)_2$. However, the X-ray diffractogram of the EAF-Slag present very complex XRD pattern shown in Fig 2b. It seems that different mineral phases with distinct peaks of high intensities and some overlapping peaks of low intensities were detected. The slow cooling conditions of the EAF-Slag allow the formation of various crystalline phases. The primary ones being: Magnetite (Ref. PDF#08-0479), Calcite (Ref. PDF#86-2339), Siderite (Ref. PDF#83-1764), Gehlenite (Ref. PDF#87-0968), Wustie (Ref. PDF#06- 0615) and Calcium Silicate (Ref. PDF#20-0237) [13].

TABLE 1: Chemical composition of precursors as determined by EDX analysis.

Oxides (% mass)	EAF-slag	TMWM
CaO	33.29	0.69
SiO_2	15	46.67
Al_2O_3	10.08	17.05
Fe_2O_3	30.48	15.47
MgO	4.54	4.83
Na_2O	0.13	0.85
P_2O_5	0.21	-
SO_3	0.19	7.9
TiO_2	0.82	0.6
Ba	0.05	-
Cr	2.08	-
Mn	3.13	-
ZnO	-	1.09
K_2O	-	4.85

2.1.2. Alkaline Activators

Analytical grade sodium hydroxide (NaOH with 98% purity, supplied by Fisher Scientific, Schwerte, Germany) flakes dissolved in deionized water with a concentration of 10M, the activator solution was prepared at least one day prior to its use.

Sodium silicate solution (ref.D40), supplied by Solvay SA, Póvoa de Santa Iria, Portugal) SiO_3/Na_2O = 3.23 (8.60% by weight Na_2O, 27.79% by weight SiO_2, 63.19% by weight H_2O, and 0.4% by weight Al_2O_3). were used. Both alkaline activators were mixed together using Magnetic stirrers " agimatic and selecta" for period of 5 min with (Na_2SiO_3/NaOH) ratio 4/1.

-a) TMWM

Q: Quartz
M: Muscovite
C: Clinochlore

-b) EAF-Slag

Mg: Magnesite ; Ca: Calcite
Si: Siderite   ; Ge: Gehlenite
Wu: Wustite ;   CS: Calcium
Silicate
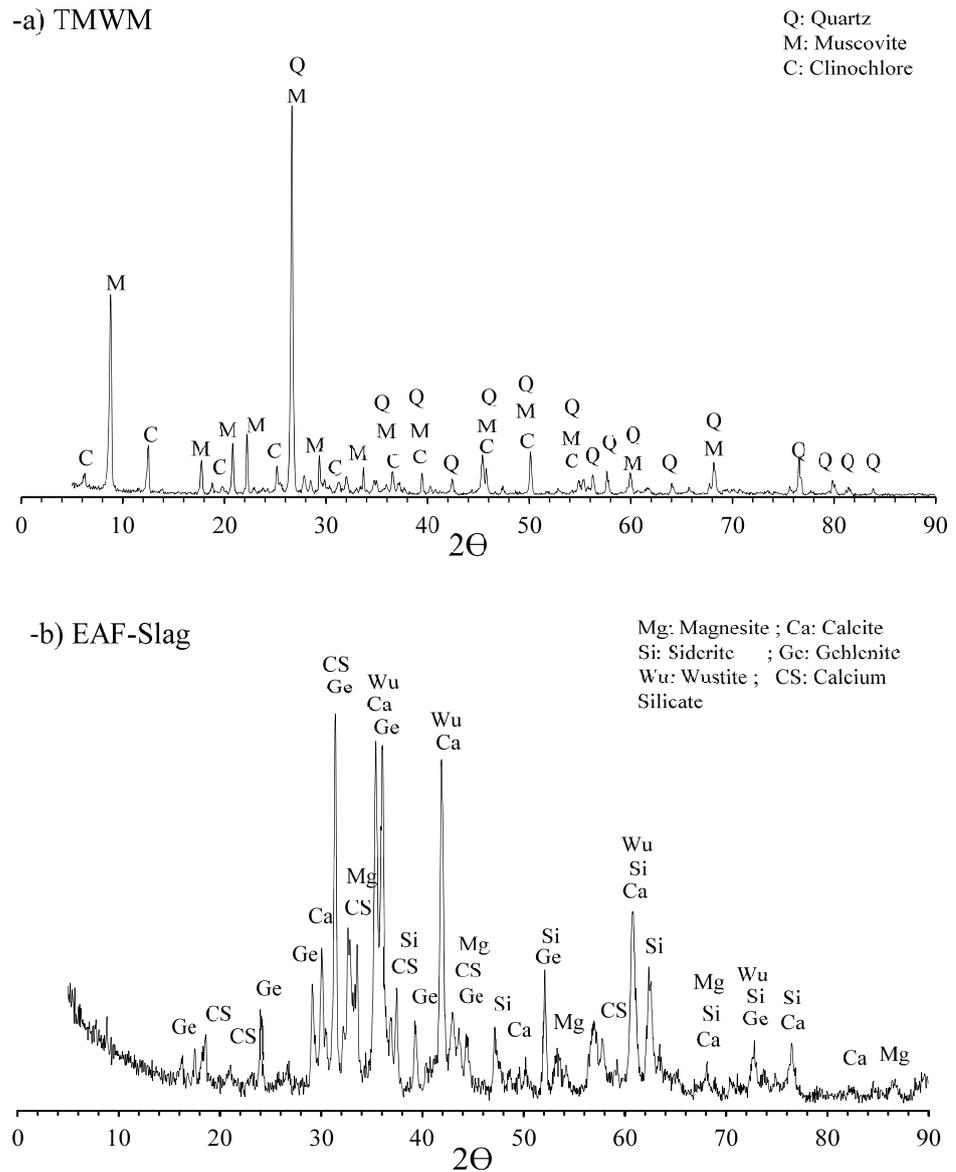
Figure 2: X-ray diffraction pattern of both raw materials (TMWM and EAF-Slag).

2.2. Processing, molding and curing

The TMWM powder with up to 50% by mass replacement with EAF-Slag were hand blended for 60 s. The low liquid-to-solid binary TMWM-EAF-Slag alkali-activated material mixtures were made by mixing the raw powders with an alkaline activator solution (12.5% alkaline activator solution calculated from the total weight of the precursor) for about 180 s. The liquid-to-solid ratio (*L/S*) was about 11.11% from the total weight of the mixture. The mixture was cast into 20 × 20 × 20 mm lubricated cubic-shaped steel moulds, vibrated for compaction, and pressed under a pressing pressure ranging 20, 40, 60, 80, 100 MPa, and then sealed with a plastic sheet as to minimize loss of evaporable

water. Afterwards the samples were left to cure undisturbed at 60 °C for 24 h, and then air cured at room temperature up to 7,14 and 28 days and then exposed to compressive strength measurements. Besides, the resulted sample fragments were milled and sieved under 75 µm, after subjected for FT-IR.

2.3. Tests

To investigate the strength-microstructure relationship, the crashed samples came from compressive strength tests taken from the debris, milled and sieved under 75 µm for FTIR investigation.

- The compressive strength tests were investigated using a 3000 kN electro-hydraulic mechanical testing machine "ADR Touch 3000 BS EN Compression Machine with Digital Readout and Self Centring Platens", as specified in European standard EN 196-1. A set of five specimen cubes were tasted in each case and the average value of these five were reported. Compressive strength data was collected using 20 mm cubic size specimens.

- FT-IR analysis was carried out using Nicolet iS10 FTIR Spectrometer (Thermo Scientific), Smart iTR accessory instrument in transmittance mode at frequencies (4000-600 cm^{-1}).

3. Results and Discussion

3.1. Compressive strength development

The compressive strengths of the low liquid-to-solid binary TMWM-EAF-Slag alkali-activated compressed material pastes using different increasing pressures (20, 40, 60, 80 and 100 MPa) cured for 7, 14 and 28 days are shown in Fig 3. Note that the compressive strengths of the specimens are increased with the increase of the compression pressure applied on the pastes. In-depth details, the compressive strength increased by 76% with the increased load from the lowest compression pressure load value 20 MPa to the highest load value 100 MPa. The maximum compressive strength (50.57 MPa) was achieved at high compression pressure load of 100 MPa. However, the minimum compressive strength (27.60 MPa) was achieved at low compression pressure load of 20 MPa. In addition, the compressive strength increased with the increase of curing ages. The compressive strengths of the pastes cured for 7 days pressed with 20 MPa of compression pressure reached 24.13 MPa which shows a slight variation

and gain of 14.4% of strength to reach 27.6 MPa after 28 days of cure. However, the specimens prepared with a high compression pressure (100 MPa) showed, at 7 days, a compressive strength result 42.47 MPa slightly increased by 19.1% to reach 50.57 MPa after 28 days. During the curing period from 7 to 28 days, the samples compacted with the highest compression pressure improved the compressive strength (19.1% of compressive strength developed), compared with those made with lower compacting pressure (14.4% of compressive strength developed).
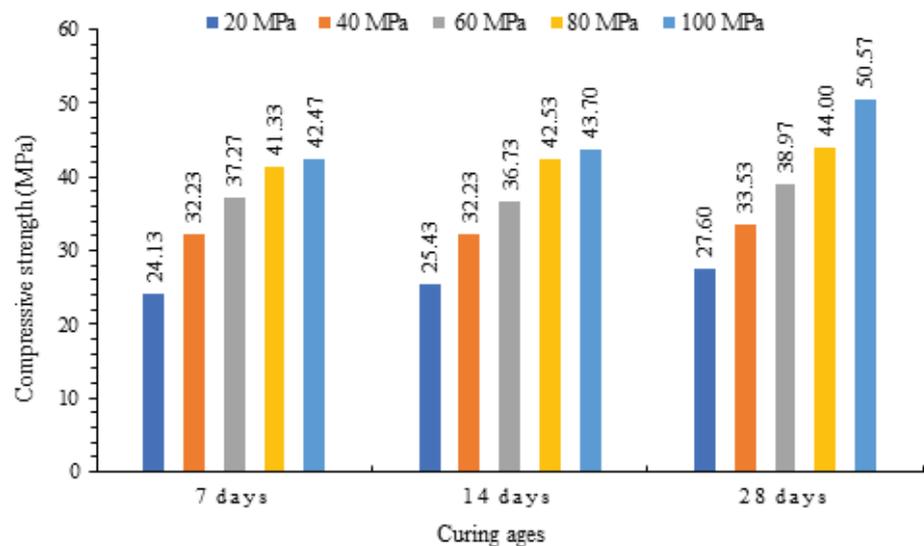
Figure 3: Compressive strength of the low liquid-to-solid binary TMWM-EAF-Slag alkali-activated materials at intensification compressing pressures at 7, 14 and 28 days.

3.2. FT-IR analysis

Fig 4 shows the FTIR spectra of the low liquid-to-solid binary TMWM-EAF-Slag alkali-activated material, made by applying a different increasing compression pressure (20, 40, 60, 80 and 100 MPa) on the samples. In the current FTIR spectra the main absorption wavenumbers bands were as follows: 1473, 1462, 1380, 1251, 1155, 1082, 956, 827 and 799 cm^{-1}. The intensities of the initial peaks (799 cm^{-1}) symmetric stretching vibration of (Si-O-Si) remained unchanged after the alkaline activation of the binary low-liquid-to-solid alkali-activated material specimens despite the increasing of the compression pressure attributed to α-quartz at about 799 cm^{-1}. Besides, the peaks at 827 cm^{-1} typical for the presence of calcium carbonate phases (the out-of-plane bending of the C-O bond) correspond to calcite content in EAF-S [18–19]. Through the examination of the FTIR spectra of TMWM-EAF-Slag alkali-activated samples, there was an obvious implication at the bands attributed to the asymmetric stretching vibrations of (Si-O-T)

where T is Si or Al. Specifically, the FTIR spectra for the samples showed a broad distribution of bond angles centred around two similar bond environments for each sample at wavenumbers of 956 cm^{-1} and 1155 cm^{-1} which can be attributed to Si-O-T (T = Al, Si) asymmetric stretching vibrations and Si-O-Si asymmetric stretching vibration respectively. The band intensities increase with the intensification of compressing pressure indicative of a higher degree of the aluminosilicates and calcium silicate hydrate phase networks after alkaline activation. In addition, the rise of intensity can indicate a larger presence of the Si–O vibration band generated by the SiO_4 groups in the anhydrous raw materials (TMWM and EAF-Slag) due to the formation of a calcium silicate hydrate, a (C-S-H) gel and calcium aluminosilicate hydrate, a (C-A-S-H) gel [20–22]. Therefore, shoulder bands at 1082 cm^{-1} corresponding to Si-O and Al-O vibration [23], can be associated with the formation of a silicon-rich gel with some sodium (N-A-S-H) gel in the low liquid-to-solid binary TMWM-EAF-Slag alkali-activated material composition [24–26]. This band is typical of the aluminosilicates spectra, and its frequency depends slightly on the state of hydration and the intensities of peaks which increase with the intensification of compression pressure. Higher compression pressure results of more (N-A-S-H) gel formation. The peaks at wavenumber 1082 cm^{-1} show the lowest intensities compared with other peaks corresponding to (N-A-S-H) gel, which mean that less (N-A-S-H) gel was formed in the system compared with other gels such as C-S-H and C-A-S-H gels. Meanwhile, bands at wavenumbers 1245-1249 cm^{-1} are attributed to the length as well as the angle of the Si-O and Al-O bonds in the silicates, in this case being sodium aluminosilicate (N-A-S-H) and/or calcium aluminosilicate (C-A-S-H) and probably other XRD-amorphous silicate phases [27].
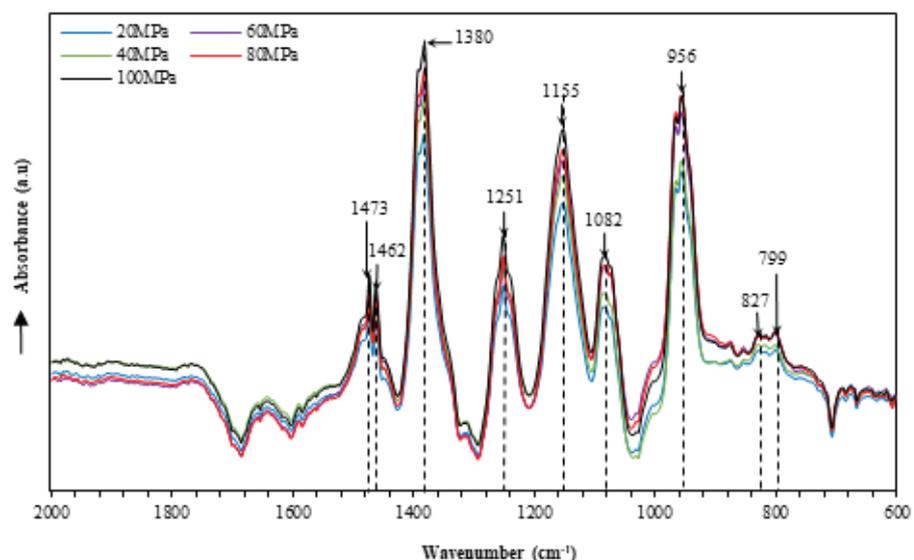
Figure 4: FT-IR spectra for asymmetric stretching (Si-O-Si and Si-O-Al) at wavenumber 950-1255 cm^{-1} and asymmetrical stretching vibration of the O-C-O) at wavenumber 1462-1473 cm^{-1}.

Additionally, the band at wavenumbers 1382 cm^{-1} related to the formation of a mixed carbonate (with alkali and alkaline earth cations) due to alkaline activation [28]. The intensities of this band are increase with the intensification of compressing pressure meaning more formation of the alkaline activation products and that more formation of carbonate. Moreover, bands typical of carbonate phases are seen at 1462 and 1473 cm^{-1}. These bands are related with the presence of calcite ($CaCO_3$) and sodium carbonate (Na_2CO_3). All the samples show similar carbonate band intensity.

This is attributed to $CaCO_3$ content in the samples (contained in EAF-Slag as crystalline phase) which remain unreacted despite the rise of the compression pressures. Besides, a small amount of Na_2CO_3 formation can occur due to the reaction of NaOH with atmospheric CO_2 in all the samples during the curing process at the laboratory in open air. As a conclusion, the results of FT-IR spectra obtained for low liquid-to-solid binary TMWM-EAF-Slag alkali-activated material pastes are in agreement with those of compressive strength of the hardened pastes where the intensity of aluminosilicate bands increase with the intensification of compression pressure.

4. Conclusions

The current study investigates the effect of the different compression pressures applied on the low liquid-to-solid binary TMWM-EAF-Slag alkali-activated samples. the compressive strength and the FT-IR spectra of low liquid-to-solid binary TMWM-EAF-Slag alkali-activated material. The following conclusions may be drawn:

- The compressive strength of the low liquid-to-solid binary TMWM-EAF-Slag alkali-activated material increase with the intensification of compressing pressure applied on the samples, which enhances the performance and the properties of the materials.

- A positive correlation between the compression pressure and the compressive strength gain was found. Regardless the compression pressure applied, on the samples, the compressive strength is developed over time.

- The absorbance intensities of the asymmetric stretching (Si-O-Si and Al-O-Si) bands from FT-IR of the samples increase with the intensification of the compression pressures from 20 to 100 MPa. It can be deduced that with the increase of intensities there is a growth of the amorphous content of calcium silicate hydrate

(C-S-H) gel, calcium aluminosilicate hydrates (C-A-S-H) gel and sodium aluminosilicate hydrate (N-A-S-H) gel, which has a positive effect on the enhancement of compressive strength results.

- The carbonates calcite ($CaCO_3$) and sodium carbonates (Na_2CO_3) which resulted from the atmospheric reaction between the unreacted Na cation with the atmosphere are the same in all the samples, as detected by the asymmetrical stretching vibration of the (O-C-O). In addition, the mineral phases (such as calcite and quartz) remain as unreacted components which are unaffected by the intensification of the compression pressures.

Acknowledgements

References

[1] R. M. Andrew, Global CO2 emissions from cement production. *Earth System Science Data Discussions*, (2017) 1–52.

[2] L. Huang, G. Krigsvoll, F. Johansen, Y. Liu, & X. Zhang, Carbon emission of global construction sector. *Renewable and Sustainable Energy Reviews*, **81** (2018) 1906–1916.

[3] J.. Provis & J. S. J. Van Deventer, *Geopolymers - Structure, processing, properties and industrial applications* (Woodhed Publishing Limited and CRC Press LLC, 2009).

[4] D. Panias, I. P. Giannopoulou, & T. Perraki, Effect of synthesis parameters on the mechanical properties of fly ash-based geopolymers. *Colloids and Surfaces A: Physicochemical and Engineering Aspects*, **301** (2007) 246–254.

[5] H. Xu & J. S. Van Deventer, Microstructural characterisation of geopolymers synthesised from kaolinite/stilbite mixtures using XRD, MAS-NMR, SEM/EDX, TEM/EDX, and HREM. **32** (2002) 1705–1716.

[6] N. Sedira, J. Castro-Gomes, G. Kastiukas, X. Zhou, & A. Vargas, A review on mineral waste for chemical-activated binders: mineralogical and chemical characteristics. *Mining Science*, **24** (2017).

[7] F. Pacheco-Torgal, J. P. Castro-Gomes, & S. Jalali, Investigations of tungsten mine waste geopolymeric binder: Strength and microstructure. *Construction and Building Materials*, **22** (2008) 2212–2219.

[8] N. Sedira and J. Castro Gomes, "Strength and microstructure of tungsten mining waste-based hybrid alkaline material: effect of activators," in Proceedings of the 12th fib International PhD Symposium in Civil Engineering, 2018, pp. 145–152.

[9] G. Kastiukas, D. Ph, X. Zhou, D. Ph, M. Asce, & J. Castro-gomes, Preparation Conditions for the Synthesis of Alkali-Activated Binders Using Tungsten Mining Waste. **29** (2017) 1–9.

[10] N. Sedira, J. Castro-Gomes, & M. Magrinho, Red clay brick and tungsten mining waste-based alkali-activated binder: Microstructural and mechanical properties. *Construction and Building Materials*, **190** (2018) 1034–1048.

[11] A. Palomo, M. W. Grutzeck, & M. T. Blanco, Alkali-activated fly ashes: A cement for the future. *Cement and Concrete Research*, **29** (1999) 1323–1329.

[12] W. Gutt & P. J. Nixon, Use of waste materials in the construction industry. *Matériaux et Construction*, **12** (1979) 255–306.

[13] N. Sedira & J. Castro-gomes, Effects of EAF-S on alkali-activation of tungsten mining waste: mechanical properties. *REMINE - Int. Conf. Brok. Event - UBI, Covilha, Portugal.* (2019), pp. 1–6.

[14] P. S. Humbert & J. Castro-Gomes, CO2 activated steel slag-based materials: A review. *Journal of Cleaner Production*, **208** (2019) 448–457.

[15] H. M. Khater & M. Ezzat, Preparation and characterization of engineered stones based geopolymer composites. *Journal of Building Engineering*, **20** (2018) 493–500.

[16] N. Sedira & J. Castro-gomes, Study of an alkali-activated binder based on tungsten mining mud and brick powder waste. *8th Scientific-Technical Conference on Material Problems in Civil Engineering*, **06002** (2018) 1–8.

[17] P. S. Humbert, J. P. Castro-Gomes, & H. Savastano, Clinker-free CO 2 cured steel slag based binder: Optimal conditions and potential applications. *Construction and Building Materials*, **210** (2019) 413–421.

[18] S. N. Ghosh, Infra-red spectra of some selected minerals, rocks and products. *Journal of Materials Science*, **13** (1978) 1877–1886.

[19] M. Criado, W. Aperador, & I. Sobrados, Microstructural and mechanical properties of alkali activated Colombian raw materials. *Materials*, **9** (2016).

[20] F. Puertas & M. Torres-Carrasco, Use of glass waste as an activator in the preparation of alkali-activated slag. Mechanical strength and paste characterisation. *Cement and Concrete Research*, **57** (2014) 95–104.

[21] P. Yu, R. J. Kirkpatrick, B. Poe, P. F. McMillan, & X. Cong, Structure of Calcium Silicate Hydrate (C-S-H): Near-, Mid-, and Far-Infrared Spectroscopy. *Journal of the American Ceramic Society*, **48** (1999) 742–748.

[22] O. Rudić, V. Ducman, M. Malešev, V. Radonjanin, S. Draganić, S. Šupić, & M. Radeka, Aggregates Obtained by Alkali Activation of Fly Ash: The Effect of Granulation, Pelletization Methods and Curing Regimes. *Materials*, **12** (2019) 776.

[23] Z. Sun, H. Cui, H. An, D. Tao, Y. Xu, J. Zhai, & Q. Li, Synthesis and thermal behavior of geopolymer-type material from waste ceramic. *Construction and Building Materials*, **49** (2013) 281–287.

[24] I. Garcıa-Lodeiro, A. Fernández-Jiménez, M. T. Blanco, & A. Palomo, FTIR study of the sol − gel synthesis of cementitious gels: C − S − H and N − A − S − H. *Journal of Sol-Gel Science and Technology*, (2008) 63–72.

[25] I. G. Lodeiro, D. E. Macphee, A. Palomo, & A. Fernández-jiménez, Effect of alkalis on fresh C − S − H gels. FTIR analysis. *Cement and Concrete Research*, **39** (2009) 147–153.

[26] N. Sedira & J. Castro-gomes, Effect of activators on hybrid alkaline binder based on tungsten mining waste and ground granulated blast furnace slag. *Construction and Building Materials*, **232** (2020) 117176.

[27] S. Onisei, Y. Pontikes, T. Van Gerven, G. N. Angelopoulos, T. Velea, V. Predica, & P. Moldovan, Synthesis of inorganic polymers using fly ash and primary lead slag. *Journal of Hazardous Materials*, **205**−**206** (2012) 101–110.

[28] C. Dupuy, A. Gharzouni, N. Texier-Mandoki, X. Bourbon, & S. Rossignol, Alkali-activated materials based on callovo-oxfordian argillite: Formation, structure and mechanical properties. *Journal of Ceramic Science and Technology*, **9** (2018) 127–140.